EPJ Web of Conferences **292**, 08006 (2024) https://doi.org/10.1051/epjconf/202429208006
*NRM2023*

# The role of angular momentum in fission

*R.* Vogt[1,2,*] and *J.* Randrup[3]

[1]Nuclear and Chemical Sciences Division, Lawrence Livermore National Laboratory, Livermore, CA, USA
[2]Physics and Astronomy Department, University of California, Davis, CA, USA
[3]Nuclear Science Division, Lawrence Berkeley National Laboratory, Berkeley, CA, USA

**Abstract.** The role of angular momentum in fission has generated a great deal of attention recently. Recent data has shown that, while the fission fragment spins may be generated by highly correlated processes, the resulting measured fragment spins were shown to be largely uncorrelated. This proceedings will summarize some of the advances made with the fission simulation model FREYA which is well suited for studying the role of angular momentum in fission because it can easily simulate a variety of scenarios for generating fragment spin and determine the observational consequences.

## 1 Introduction

Nuclear fission has been studied intensively for decades and, while much is known about certain aspects, particularly those related to applications, others have yet to be understood in detail. While many-body models of fission have developed considerably in recent years and have had some success in predicting the fragment mass yields, phenomenological models that can describe complete fission events are required to study correlated observables. There are a number of such codes available but only `FREYA` conserves both linear and angular momentum throughout a fission event. Thus `FREYA` is ideal for studying the generation of angular momentum in fission and its observational consequences.

Angular momentum in fission has been studied experimentally since the 1970s. The classic early measurement of photon angular distributions relative to the fragment motion [1, 2] suggested that the angular momentum of the primary fragments were perpendicular to the fission axis, albeit with large uncertainties. A number of more recent experiments studied neutron-photon correlations in fission [3–5], the dependence of photon emission on fragment mass and total kinetic energy [3, 6, 7], and fragment spin correlations based on rotational transitions [8]. The latter measurement found that the average spin of one fragment was practically independent of the minimum spin of the other fragment, concluding there was no significant correlation between the fragment spins and the fragment spins must be generated after scission and thus after the fragments have become two separate, independent systems [8]. Such a mechanism would seem to violate angular momentum conservation.

`FREYA` calculations show that even though the fragment spins start out highly correlated, population of both positive and negative rotational modes decorrelates the spins. This proceeding introduces `FREYA`, discusses the character of these modes, and describes how studies of photon angular distributions can determine their relative excitation.

*e-mail: rlvogt@lbl.gov

## 2 Introduction to FREYA

Here the basic outline of how FREYA models a fission event is presented, with an emphasis on the parts related to angular momentum. FREYA requires the mass distribution of the primary fission fragments, $Y(A)$, and the mean total kinetic energy for a given mass split, $\overline{\mathrm{TKE}}(A)$, for the particular system. FREYA can also be configured to accept other yields [9, 10].

The initial compound nucleus $A_0$ splits into light and heavy fragments, $A_L$ and $A_H$. One fragment is sampled from $Y(A)$, assuming binary fission. The other fragment is determined by mass and charge conservation and the fission $Q$-value is calculated. The TKE is taken from $\mathrm{TKE}(A_H)$ to obtain the total excitation energy available for rotational and statistical excitation at scission, $E^*_{\mathrm{sc}} = Q - \overline{\mathrm{TKE}}$. The corresponding 'scission temperature' $T_{\mathrm{sc}}$ is obtained from $E^*_{\mathrm{sc}} = a(A_0)T^2_{\mathrm{sc}}$ with the level density parameter $a(A) \propto A/e_0$ where $e_0 \approx 10$ MeV.

In addition to any overall rigid rotation of the fissioning system, which determines the mean fragment angular momenta, there are also fluctuations around these mean values due to the wriggling and bending modes, as discussed in Sec. 3. Assuming these modes are fully excited, the magnitude of these spin fluctuations is governed by the 'spin temperature' $T_S = c_S T_{\mathrm{sc}}$ with parameter $c_S$.

After subtracting the rotational energy of the two fragments, $E_{\mathrm{rot}}$, $E_{\mathrm{stat}} = E^*_{\mathrm{sc}} - E_{\mathrm{rot}}$ is left for statistical excitation and is partitioned between the two fragments employing their heat capacities and a parameter $x$ that gives more excitation energy to the light fragment.

After the mean fragment excitation energies have been assigned, FREYA considers thermal fluctuations in the statistical excitation. An energy fluctuation $\delta E^*_i$ is sampled from a truncated gaussian distribution of variance $2c\overline{E}^*_i T_i$ and the fragment excitations are adjusted accordingly, $E^*_i = \overline{E}^*_i + \delta E^*_i$, $i = L, H$. Energy is conserved by making a compensating opposing fluctuation in TKE, $\mathrm{TKE} = \overline{\mathrm{TKE}} - \delta E^*_L - \delta E^*_H$. Finally, TKE may be adjusted by the FREYA parameter, $d\mathrm{TKE}$, to reproduce the average neutron multiplicity, $\overline{\nu}$.

Once the fragment initial conditions have been assigned, neutron and photon emission follow. Neutrons are evaporated isotropically in the frame of the emitting fragment, apart from a slight flattening due to fragment rotation. The neutron kinetic energy is sampled from a black-body spectrum. FREYA assumes that neutron evaporation continues until the fragment excitation energy is below the neutron separation energy $S_{\mathrm{n}}$.

After neutron evaporation has ceased, photons are emitted. Statistical photons are first emitted isotropically with an energy distribution sampled from a black-body spectrum modulated by a giant-dipole resonance form factor. When the remaining nuclear excitation energy is in the range of RIPL-3 compilation [11], FREYA switches to a discrete cascade which is continued until the half-life of the state exceeds a specified value, $t_{\mathrm{max}}$, based on the detector response time, or until the nucleus is in its ground state.

## 3 Rotational modes in the dinucleus

As the fissioning system approaches scission, it acquires a binary character, eventually consisting of two proto-fragments in close proximity with their nucleon numbers, $(Z_L, N_L)$ and $(Z_H, N_H)$, frozen in. These two proto-fragments are in relative motion with angular momentum $\boldsymbol{L} = \boldsymbol{R} \times \boldsymbol{P}$. Here $\boldsymbol{R} \equiv \boldsymbol{R}_L - \boldsymbol{R}_H$ is the relative position of the light and heavy proto-fragments with the direction of $\boldsymbol{R}$ at scission defining the fission axis. The relative fragment momentum is $\boldsymbol{P} = \mu(\boldsymbol{V}_L - \boldsymbol{V}_H)$ where $\boldsymbol{V}_i$ is the velocity of fragment $i$ and $\mu \approx mA_LA_H/(A_L + A_H)$ is the reduced mass of the fragments. The individual proto-fragments also generally have angular momenta, $\boldsymbol{S}_L$ and $\boldsymbol{S}_H$, giving a total angular momentum of the binary system of $\boldsymbol{S}_0 = \boldsymbol{S}_L + \boldsymbol{S}_H + \boldsymbol{L}$. Both the total linear momentum, $\boldsymbol{P}_0 \approx m(A_L\boldsymbol{V}_L + A_H\boldsymbol{V}_H)$,

and total angular momentum, $\boldsymbol{S}_0$, are conserved. The fissioning system undergoes an overall rigid rotation with angular momentum $\boldsymbol{S_0}$. This rotation is typicall negligible in low energy fission and is absent in $^{252}$Cf(sf).

The angular-momentum modes can be conveniently rewritten in normal form [12–14],

$$E_0^{\rm rot} = \frac{S_L^2}{2\mathcal{I}_L} + \frac{S_H^2}{2\mathcal{I}_H} + \frac{(\boldsymbol{S}_0 - \boldsymbol{S}_L - \boldsymbol{S}_H)^2}{2\mathcal{I}_R} = \frac{S_0^2}{2\mathcal{I}_0} + \frac{s_{\rm wrig}^2}{2\mathcal{I}_{\rm wrig}} + \frac{s_{\rm bend}^2}{2\mathcal{I}_{\rm bend}} + \frac{s_{\rm twst}^2}{2\mathcal{I}_{\rm twst}} + \frac{s_{\rm tilt}^2}{2\mathcal{I}_{\rm tilt}} \quad (1)$$

where $\mathcal{I}_L$ and $\mathcal{I}_H$ are the moments of inertia of the individual fragments, $\mathcal{I}_R = \mu R^2$ is the moment of inertia for the orbital motion, and $\mathcal{I}_0 = \mathcal{I}_L + \mathcal{I}_H + \mathcal{I}_R$ is the total moment of inertia. The normal modes [12]: wriggling, bending, twisting and tilting, are discussed in turn.

The rotational energy in Eq. (1) is minimized when none of the normal modes are agitated, leaving only rigid rotation. The normal modes, carrying no net angular momentum, make fluctuating contributions on top of rigid rotation. The wriggling and bending modes, assumed to be fully agitated in the default version of `FREYA`, are perpendicular to the fission axis while the twisting and tilting modes are parallel to it. The contributions of the fluctuating modes dominate over rigid rotation [15].

The wriggling contributions, perpendicular to the fission axis $\boldsymbol{R}$, are parallel to each other,

$$\delta\boldsymbol{S}_{L,H}^{\rm wrig} = ((\mathcal{I}_{L,H})/(\mathcal{I}_L + \mathcal{I}_H))\boldsymbol{s}_{\rm wrig}\ , \quad \delta\boldsymbol{L}^{\rm wrig} = -\boldsymbol{s}_{\rm wrig}\ , \quad (2)$$

with $\mathcal{I}_{\rm wrig} = (\mathcal{I}_L + \mathcal{I}_H)\mathcal{I}_R/\mathcal{I}_0$ in Eq. (1). The change in $\boldsymbol{L}$ is required by angular momentum conservation which also reduces the moment of inertia by $\mathcal{I}_R/\mathcal{I}_0$. Because the space perpendicular to $\boldsymbol{R}$ is two dimensional, there are two independent, degenerate wriggling modes.

The bending contributions, also perpendicular to the fission axis, are opposite each other,

$$\delta\boldsymbol{S}_L^{\rm bend} = \boldsymbol{s}_{\rm bend}\ , \quad \delta\boldsymbol{S}_H^{\rm bend} = -\boldsymbol{s}_{\rm bend}\ , \quad \delta\boldsymbol{L}^{\rm bend} = \boldsymbol{0}\ , \quad (3)$$

with $\mathcal{I}_{\rm bend} = \mathcal{I}_L\mathcal{I}_R/(\mathcal{I}_L + \mathcal{I}_R)$ in Eq. (1). Because the bending contributions to the fragment spins are equal and opposite, bending has no effect on $\boldsymbol{L}$. Similar to wriggling, the two bending modes are independent and degenerate.

The twisting contributions are parallel to the fission axis and opposite, $\boldsymbol{s}_{\rm twst} = s_{\rm twst}\hat{\boldsymbol{R}}$,

$$\delta\boldsymbol{S}_L^{\rm twst} = \boldsymbol{s}_{\rm twst}\ , \quad \delta\boldsymbol{S}_H^{\rm twst} = -\boldsymbol{s}_{\rm twst}\ , \quad \delta\boldsymbol{L}^{\rm twst} = \boldsymbol{0}\ , \quad (4)$$

with $\mathcal{I}_{\rm twst} = \mathcal{I}_{\rm bend}$ in Eq. (1).

In the tilting mode, the spins are also parallel to the fission axis, $\boldsymbol{s}_{\rm tilt} = s_{\rm tilt}\hat{\boldsymbol{R}}$,

$$\delta\boldsymbol{S}_i^{\rm tilt} = (\mathcal{I}_i/\mathcal{I}_{\rm tilt})\boldsymbol{s}_{\rm tilt}\ , \quad \delta\boldsymbol{L}^{\rm tilt} = -\boldsymbol{s}_{\rm tilt}\ , \quad (5)$$

with $\mathcal{I}_{\rm tilt} = \mathcal{I}_L + \mathcal{I}_H$ in Eq. (1). Because the system is isolated, tilting is not directly excited but appears only because the orbital plane of motion is tilted in response to wriggling recoils perpendicular to $\boldsymbol{L}$. Thus the timescale for tilting is long [14] and it can be ignored.

The angular momenta of the emerging fragments is built up of contributions from the normal rotational modes where the two spins in each mode are highly correlated. Models of fission fragment spins differ in the degree to which they are populated. In the thermal limit, the modes are populated statistically so that the distributions of the spin fluctuations of mode $m$ are $P_m(s_m) \sim \exp(-s_m^2/2\mathcal{I}_m T)$ with corresponding variance $\langle s_m^2\rangle_T = \mathcal{I}_m T$, where $T$ is the effective temperature [13]. Whether the statistical limit is realized depends on the characteristic timescales of the agitation of those modes.

Each of the normal modes has a relaxation time, $t_m$, the time scale over which the mode equilibrates. If $t_m$ is significantly shorter than the fission time, the mode should be in equilibrium at scission. Otherwise it is not. The rotational time scales were derived on the basis

of the nucleon exchange transport model [16, 17]. Although it was developed for damped nuclear reactions [18, 19], the basic physics equally well applies to the late stages of fission when the binary proto-fragments have been formed.

The relaxation time for mode $m$ is $t_m = \mathcal{I}_m/M_m$, where $\mathcal{I}_m$ is the moment of inertia for each mode and $M_m$ is its mobility coefficient, derived [14] based on nucleon exchange [17],

$$M_{\rm wrig} = m\mathcal{N}R^2\ , \quad M_{\rm bend} = m\mathcal{N}\left[\left(\frac{\mathcal{I}_H R_L - \mathcal{I}_L R_H}{\mathcal{I}_L + \mathcal{I}_H}\right)^2 + c_{\rm ave}^2\right]\ , \quad M_{\rm twst} = m\mathcal{N}c_{\rm ave}^2\ . \tag{6}$$

The rate of nucleon transfers between fragments is given by $\mathcal{N} \approx \frac{1}{4}\rho\bar{v}\pi c^2$ [20] where $\rho$ is the nucleon density, $\bar{v} = \frac{3}{4}v_F$ is the mean nucleon speed, $c_{\rm ave}^2 = \frac{1}{2}c^2$ is the average value of the neck radius $c$ squared, and $R = R_L + R_H + 4$ fm. $M_{\rm twst}$ is an order of magnitude smaller than $M_{\rm wrig}$ because $R^2 \gg c^2$, giving $t_{\rm twst} \gg t_{\rm wrig}$. The first term in $M_{\rm bend}$ vanishes for symmetric splits, with $M_{\rm bend} = M_{\rm twst}$. $M_{\rm bend}$ is significantly larger than $M_{\rm twst}$ for typical asymmetric mass splits and small $c$. The relaxation times are shown in Fig. 1 as a function of $c$.

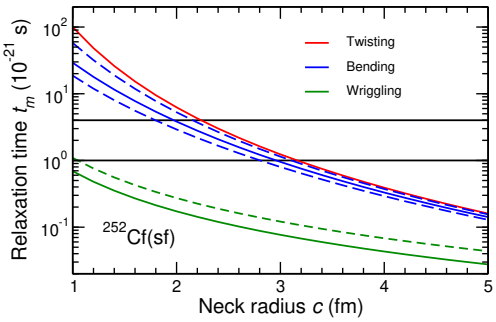


**Figure 1.** The calculated relaxation times $t_m$ for wriggling (bottom curve, green), bending (middle three curves, blue), and twisting (top curve, red), shown as functions of the neck radius $c$ for $d = 4$ fm. The wriggling result is also shown for touching spheres, $d = 0$ (dashed green). The bending curves show the most probable mass split (108:144, solid) and two half as probable splits (100:152, lower dashed, and 118:134, upper dashed). The horizontal lines show $t_{\rm fiss} = 1$ and $t_{\rm fiss} = 4 \times 10^{-21}$ s.

The relaxation times are compared with $t_{\rm fiss}$, the time needed for the fissioning system to evolve from the first appearance of the proto-fragments to the neck rupture. Because $t_{\rm fiss}$is difficult to measure experimentally, it is not well known [21, 22]. We assume that $t_{\rm fiss}$ is between one to a few $10^{-21}$ s. As seen in Fig. 1, the calculated $t_{\rm wrig}$ is well below $t_{\rm fiss}$. Thus the wriggling mode is likely to stay equilibrated until the scission time when $c \approx 2$ fm.

In contrast, $t_{\rm twst}$ is similar to or longer than $t_{\rm fiss}$. If the rotational modes are not strongly agitated, as in spontaneous fission, twisting may not be built up prior to scission. Twisting should become more important for induced fission as the excitation energy is increased.

The bending contribution is more difficult to predict without a more precise estimate of $t_{\rm fiss}$. However, if $c \approx 2$ fm and $t_{\rm fiss}$ is several times $10^{-21}$ s, bending may be appreciably agitated. The results in Wilson *et al.* [8] suggest that the spin magnitudes of the fragments are fairly independent, limiting the possible suppression of the bending mode. Because the bending contribution increases with the asymmetry of the mass split, see Eq. (6), its contribution could be studied as a function of the mass yields.

Based on these estimates, the wriggling modes should be fully equilibrated at scission while bending should be partially, if not fully, equilibrated. Twisting may be present but should not be a major contribution.

## 4 Event-by-event simulation

The angular momentum treatment described in the previous section has been incorporated into FREYA [23–25]. At scission, each of the normal modes $m$ is sampled from a Boltzmann distribution with effective temperature $T_m = c_m T_{\rm sc}$. Thus the distribution of the mode amplitude $s_m$ is $P(s_m) \sim \exp(-s_m^2/2\mathcal{I}_m T_m)$ with $c_m = (c_{\rm wrig}, c_{\rm bend}, c_{\rm twst})$. The default version of FREYA uses $c_S = c_m = (1, 1, 0)$ [24, 25]. Here, the coefficients for the modes are separated and adjusted individually to explore different degrees of agitation. When other proportions are employed, the coefficients $\{c_m\}$ are renormalized to ensure that the average fragment spin magnitudes remain unchanged.

After scission, the primary fission fragments separate along Coulomb trajectories. The associated rotation of the dinuclear axis $\boldsymbol{R} \equiv \boldsymbol{R}_L - \boldsymbol{R}_H$ is only a couple of degrees [25], so that the fragments move approximately along the fission axis. Subsequently, each fragment evaporates neutrons and photons, as described in Sec. 2.

Photon radiation is emphasized with a simplified description to enhance the physical effects discussed here. If these turn out to be sufficiently promising to warrant experimental investigations, more refined treatments should be developed.

FREYA treats neutron evaporation classically, leaving the resulting product nucleus with a classical spin vector $\boldsymbol{S}$. The spin magnitude $S \equiv |\boldsymbol{S}|$ is replaced here by a discrete integer or half-integer value $J$ according to whether the product mass number $A$ is even or odd. Further, it is assumed that the post-evaporation fragment is in a quantum state maximally aligned along the spin direction $\hat{\boldsymbol{S}}$, so the initial state, before the photon cascade, is given by $|i\rangle = |J, M = J\rangle$ when $\hat{\boldsymbol{S}}$ is the quantization axis.

In its ground state, the product nucleus angular momentum may be directed along its symmetry axis with magnitude denoted by $K_{\rm gs}$. The possible values of $J$ are then $J = K_{\rm gs}, K_{\rm gs} + 1, \ldots$ and the associated rotational energy is

$$E_{\rm rot} \;=\; [J(J+1) - K_{\rm gs}(K_{\rm gs}+1)]/\mathcal{I}_\perp(A)\,, \tag{7}$$

which vanishes in the ground state, $E_{\rm rot}^{\rm gs} = 0$. The moment of inertia is assumed to be 50% of its rigid value for simplicity, $\mathcal{I}_\perp(A) = 0.5 \times \frac{2}{5} m A R_A^2$. The statistical excitation energy of the product nucleus is then $E_{\rm stat} = E_{\rm tot} - E_{\rm rot}$, where $E_{\rm tot}$ denotes the total excitation of the mother state. As in the standard FREYA treatment, the nucleus is assumed to first dispose of its statistical excitation energy through a sequence of E1 dipole photon emissions, The simulation of the E1 cascades is carried out with a recently developed semi-classical method [26] that replaces the daughter state with a state that is also maximally aligned but along a direction that may be tilted relative to that of the mother state. The E1 cascades continue until the nucleus has reached the yrast line. For even-even nuclei, $K_{\rm gs}$ vanishes and the yrast states have even $J$ values only, $J = 0, 2, 4 \ldots$.

## 5 Spin correlations

As discussed above, the two fragment spins are not independent, due to angular momentum conservation. The spin contributions from the two fragments due to wriggling are perfectly parallel, while the contributions from bending are anti-parallel. When these modes are populated statistically, the correlation coefficient for the individual fragment spins is $c(\boldsymbol{S}_L, \boldsymbol{S}_H) \equiv [\langle \boldsymbol{S}_L \cdot \boldsymbol{S}_H\rangle - \langle \boldsymbol{S}_L\rangle\langle \boldsymbol{S}_H\rangle]/[\sigma_L \sigma_H] = -\{\mathcal{I}_L \mathcal{I}_H/[(\mathcal{I}_R + \mathcal{I}_L)(\mathcal{I}_R + \mathcal{I}_H)]\}^{1/2}$. This quantity is generally rather small because the moment of inertia for the relative fragment motion, $\mathcal{I}_R$, is typically an order of magnitude larger than $\mathcal{I}_L$ and $\mathcal{I}_H$, $\mathcal{I}_R \gg \mathcal{I}_f$. Thus, even though the fragment spins are strongly coupled for each of the normal modes, the resulting spins are

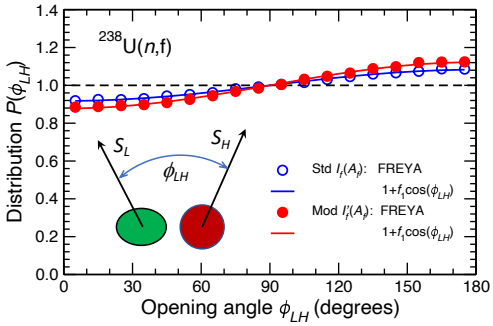


**Figure 2.** The opening angle distribution $\phi_{LH}$ between the angular momenta of two fission fragments from $^{238}$U($n$,f) obtained by FREYA using either the standard moment of inertia, $\mathcal{I}_f(A_f) = 0.5\,\mathcal{I}_{\rm rigid}(A_f)$ (dots) or a modified form depending on the shapes of the fragments at scission, $\mathcal{I}'_f(A_f)$ (open circles). Also shown are the lowest-order Fourier approximations, $P(\phi_{LH}) = 1 + f_1 \cos\phi_{LH}$. From Ref. [15].

expected to be relatively independent. This expectation is indeed borne out by actual FREYA simulations [27], as illustrated in Fig. 2.

The magnitudes of the fragment spins, $S_f = |\boldsymbol{S}_f|$, have average values $\overline{S}_f \equiv \langle S_f \rangle \approx 5-6\,\hbar$ with associated covariance $\sigma(S_L, S_H) = \langle S_L S_H \rangle - \overline{S}_L \overline{S}_H$. The spin magnitude correlation coefficient is $c(S_L, S_H) = \sigma(S_L, S_H)/[\sigma(S_L)\sigma(S_H)]$. The correlation coefficients are essentially zero, see Ref. [15], indicating that the primary spin magnitudes are largely uncorrelated, in accordance with Ref. [8].

While the experimental data [8] cannot provide information on the fragment spin directions, we note that those are also largely uncorrelated in FREYA. The degree of correlation between the fragment spin directions is brought out by the distribution of the opening angle between the two fragment spins, $\phi_{LH}$, given by $\cos\phi_{LH} = \boldsymbol{S}_L \cdot \boldsymbol{S}_H/[S_L S_H]$. This function is shown in Fig. 2 for $^{238}$U($n$,f). As was shown recently [27], the undulation of the fragment spin opening angle is generally well represented by the first harmonic, $P(\phi_{LH}) \approx 1 + f_1 \cos\phi_{LH}$ where $f_1$ is on the order of 10%, showing that the spin directions are also largely uncorrelated.

## 6 Angular distribution of collective photons

This study concentrates on sequential emission of collective E2 photons along the ground-state band in even-even product nuclei. In such processes, when the mother state is maximally aligned, the daughter state is also. Emission does not change the alignment direction of the nuclear spin but only reduces its magnitude by $2\hbar$. All photons emitted in each collective cascade are mutually uncorrelated with the same angular distribution.

The angular distribution of a photon emitted from a maximally aligned state $|J, J\rangle$ has a simple expression in polar coordinates $(\theta, \phi)$, defined relative to the quantization axis (spin direction). Generally, the distribution is azimuthally symmetric around the spin direction so that the distribution of stretched E2 transitions as a function of $\theta$ is

$$P^2_{2,h}(\theta) \;=\; \tfrac{5}{2}\left(d^2_{2,h}(\theta)\right)^2 \;=\; \tfrac{5}{8}(1 + h\cos\theta)^2 \sin^2\theta\,, \tag{8}$$

where $d^2_{2,h}(\theta)$ is a Wigner $d$-function and $h$ is the photon helicity. The distribution is normalized so that $\int P^2_{2,h}(\theta)\, d\cos\theta = 1$.

We study the angular distribution of collective photons relative to the direction of motion of the fission product emitting them: photons emitted from the light product are measured relative to the direction of the light product while photons emitted from the heavy product are measured relative to the direction of the heavy product. In an actual experiment, both product nuclei in an event may not be detected. However, because the two fragments move in nearly opposite directions, it is possible to tell which product nucleus emits the photon.

The study focuses on even-even product nuclei with specific E2 transitions that stand out sufficiently clearly above the background. FREYA can include all collective photons emitted during de-excitation of the selected even-even product nuclei. While this is not possible experimentally because not all transitions can be identified or detected, this practical challenge is not prohibitive as the signal from each identified E2 transition, and from all such nuclei, is additive. Therefore, the angular distributions are averaged over all collective transitions; automatically taking into account the increased intensity of the lower transitions.

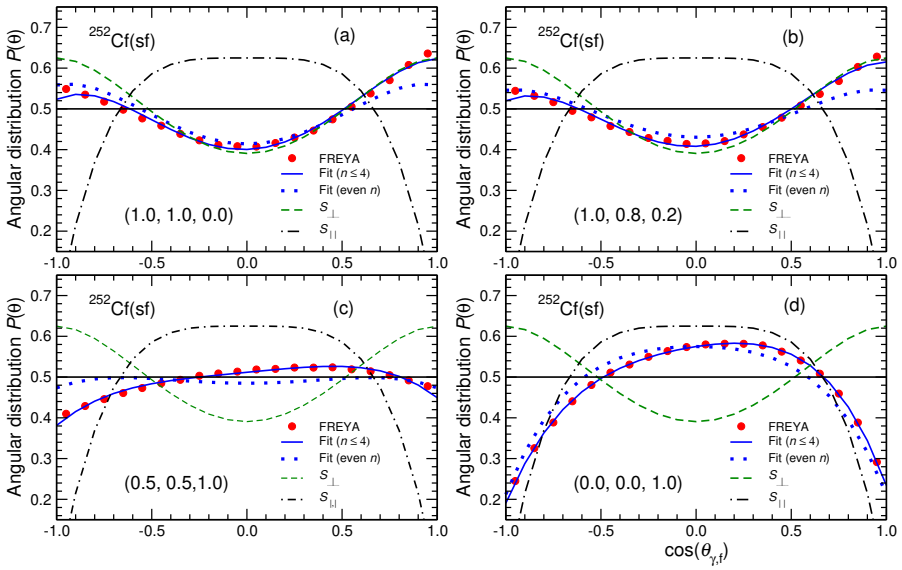


**Figure 3.** The angular distribution of the collective E2 photons relative to the direction of the emitting product nucleus for four different scenarios: The standard FREYA scenario, where the perpendicular wriggling and bending modes are fully agitated but the parallel mode (twisting) is not (a); a somewhat more realistic scenario in which bending is partially agitated while twisting is somewhat agitated (b); a less realistic scenario in which the perpendicular and the parallel modes are equally agitated (c); and an extreme scenario where only twisting is present (d). The specified values of $(c_{\mathrm{wrig}}, c_{\mathrm{bend}}, c_{\mathrm{twst}})$ are indicated for each scenario. The Legendre fits (solid curves) and their symmetric parts (dots) are shown, as are the distributions for perfectly perpendicular or perfectly parallel emitter spins. From Ref. [28].

This observable is especially interesting because it is sensitive to the direction of the angular momentum of the emitting nucleus. The angular momenta of the primary fragments are predicted to be nearly perpendicular to the fission axis at the time of scission, $\hat{\boldsymbol{R}}(t_{\mathrm{sciss}})$ as is also suggested by experiment [1, 2]. However, even if the spins were originally exactly perpendicular to $\hat{\boldsymbol{R}}(t_{\mathrm{sciss}})$, they would not be perpendicular to the direction of the asymptotic fragment motion because of the recoils from the evaporated neutrons and statistical (E1) photon emission as well as the slight Coulomb rotation.

Figure 3 shows the angular distribution $dN/d\cos\theta_{\gamma,f}$ for different assumptions about the excitation of the rotational modes, obtained by specifying the parameters $\{c_m\}$ in FREYA. For reference, the idealized distributions $P_{\parallel}(\theta_{\gamma,f})$ and $P_{\perp}(\theta_{\gamma,f})$ are shown for each scenario.

All the distributions are well represented by a fourth-order Legendre fit,

$$dN/d\cos\theta \;\sim\; 1 + A_1 P_1(\cos\theta) + \cdots + A_4 P_4(\cos\theta)\;. \tag{9}$$

While the idealized distributions $P_{\parallel}(\theta_{\gamma,f})$ and $P_{\perp}(\theta_{\gamma,f})$ are symmetric around 90°, the simulated distributions are forward skewed due to the motion of the emitting fragment relative to the laboratory frame. For the rather small fragment velocities, this focusing effect can be corrected for, to a good approximation, by retaining only the even Legendre terms.

Figure 3(a) shows the standard FREYA scenario where both the wriggling and bending modes are fully excited. Because these modes contribute spins perpendicular to the fission axis, the symmetrized distribution is therefore close to $P_{\perp}(\theta_{\gamma,f})$. The difference is due to dealignment of the spin caused by prior emissions. A somewhat more realistic scenario is shown in Fig. 3(b) where bending is not fully excited and twisting is somewhat agitated. This distribution is somewhat more isotropic but differs only slightly from the result in (a), also with a pronounced prolate appearance. Both scenarios are consistent with the data in Refs. [1, 2], albeit with large uncertainties.

Two significantly less realistic scenarios are shown in Fig. 3(c) and (d). In (c), the perpendicular and the parallel modes are equally excited. In this case, the symmetrized angular distribution is nearly isotropic. In (d), only twisting is fully agitated. As might be expected, the angular distribution now has an oblate form, similar to the idealized distribution $P_{\parallel}(\theta_{\gamma,f})$.

It may be possible to determine the degree of twisting employing the ratio $W(0°):W(90°)$, the forward relative to the sidewards yields, as illustrated in Fig. 4 where the yield ratio is shown as a function of the twisting coefficient $c_{\rm twst}$. There is a nearly linear decrease as $c_{\rm twst}$ increases from zero to one. Even the apparent small change in $dN/d\cos\theta$ in Figs. 3(a) and (b), going from no twisting to $c_{\rm twst} = 0.2$ results in a significant decrease in $W(0°):W(90°)$. Note that even though the yield ratio is quite sensitive to $c_{\rm twst}$, it is practically independent of the relative proportion of wriggling and bending: the results for three very different values of $c_{\rm bend}:c_{\rm wrig}$ are nearly identical.

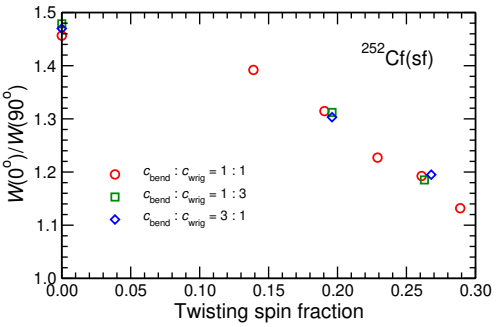


**Figure 4.** The ratio of the photon yield in the direction of the fragment, $W(0°)$, and the transverse yield, $W(90°)$, as a function of the coefficient $c_{\rm twst}$. From Ref. [28].

## References

[1] J. B. Wilhelmy *et al.*, Phys. Rev. C **5**, 2041 (1972)

[2] A. Wolf and E. Cheifetz, Phys. Rev. C **13**, 1952 (1976)
[3] T. Wang *et al.*, Phys. Rev. C **93**, 014606 (2016)
[4] S. Marin *et al.*, Phys. Rev. C **104**, 024602 (2021)
[5] S. Marin *et al.*, Phys. Rev. C **105**, 054609 (2022)
[6] A. Al-Adili *et al.*, EPJ Web Conf. **256**, 00002 (2021)
[7] M. Travar *et al.*, Phys. Lett. B **817**, 136293 (2021)
[8] J. Wilson *et al.*, Nature **590**, 566 (2021)
[9] J. Randrup, P. Talou and R. Vogt, Phys. Rev. C **99**, 054619 (2019)
[10] N. Vassh *et al.*, J. Phys. G **46**, 065202 (2019)
[11] R. Capote *et al.*, Nucl. Data Sheets **110**, 3107 (2009)
[12] J. R. Nix and W. J. Swiatecki, Nucl. Phys. **71**, 1 (1963)
[13] L. G. Moretto and R. P. Schmitt, Phys. Rev. C **21**, 204 (1980)
[14] T. Døssing and J. Randrup, Nucl. Phys. A **433**, 215 (1985)
[15] J. Randrup and R. Vogt, Phys. Rev. Lett. **127**, 062502 (2021)
[16] J. Randrup, Nucl. Phys. A **327**, 490 (1979)
[17] J. Randrup, Nucl. Phys. A **383**, 468 (1983)
[18] W. U. Schröder *et al.*, Phys. Rev. Lett. **44**, 308 (1980)
[19] W. U. Schröder and J. P. Huizenga, in Treatise On Heavy-Ion Science, edited by D.A. Bromley (Plenum, New York, 1984), p. 115
[20] J. Błocki *et al.*, Ann. Phys. **113**, 330 (1978)
[21] B. B. Back, Proceedings of the Sixth International Conference on Fission and Neutron-Rich Nuclei, Sanibel Island, Florida, Nov. 6-12, 2016, Editor, J. Hamilton, World Scientific, Singapore (2017) p. 600
[22] B. B. Back, Proceedings of 13$^{\text{th}}$ International Conference on Nucleus-Nucleus Collisions, JPS Conf. Proc. 32, 0100002 (2020)
[23] J. M. Verbeke, J. Randrup, and R. Vogt, Comp. Phys. Comm. **191**, 178 (2015)
[24] J. M. Verbeke, J. Randrup, and R. Vogt, Comp. Phys. Comm. **222**, 263 (2018)
[25] J. Randrup and R. Vogt, Phys. Rev. C **89**, 044601 (2014)
[26] J. Randrup and T. Døssing, in preparation
[27] R. Vogt and J. Randrup, Phys. Rev. C **103**, 014610 (2021)
[28] J. Randrup, T. Døssing and R. Vogt, Phys. Rev. C **106**, 014609 (2022)